Metabolic Engineering Communications 11 (2020) e00153

Contents lists available at ScienceDirect

Metabolic Engineering Communications

journal homepage: www.elsevier.com/locate/mec

Novel allosteric inhibition of phosphoribulokinase identified by ensemble kinetic modeling of *Synechocystis* sp. PCC 6803 metabolism

Hiroki Nishiguchi [a], James Liao [b], Hiroshi Shimizu [a], Fumio Matsuda [a,*]

[a] Department of Bioinformatic Engineering, Graduate School of Information Science and Technology, Osaka University, 1-5 Yamadaoka, Suita, Osaka, 565-0871, Japan
[b] Institute of Biological Chemistry, Academia Sinica, 115, Taipei, Taiwan

ARTICLE INFO

Keywords:
Synechocystis sp. PCC 6803
Allosteric regulation
Phosphoribulokinase
Ensemble kinetic modeling
Computer simulation of metabolism

ABSTRACT

The present study attempted a computer simulation of the metabolism of a model cyanobacteria, *Synechocystis* sp. PCC 6803 (PCC 6803) to predict allosteric inhibitions that are likely to occur in photoautotrophic and mixotrophic conditions as well as in a metabolically engineered strain. PCC 6803 is a promising host for direct biochemical production from CO_2; however, further investigation of allosteric regulation is required for rational metabolic engineering to produce target compounds. Herein, ensemble modeling of microbial metabolism was applied to build accurate predictive models by synthesizing the results of multiple models with different parameter sets into a single score to identify plausible allosteric inhibitions. The data driven-computer simulation using metabolic flux, enzyme abundance, and metabolite concentration data successfully identified candidates for allosteric inhibition. The enzyme assay experiment using the recombinant protein confirmed isocitrate was a non-competitive inhibitor of phosphoribulokinase as a novel allosteric regulation of cyanobacteria metabolism.

1. Introduction

The model cyanobacteria, *Synechocystis* sp. PCC 6803 (PCC 6803) is a promising host for the direct biochemical production from CO_2 (Angermayr et al., 2015; Hirokawa et al., 2017; Lai and Lan, 2015; Mohammadi et al., 2016; Oliver et al., 2016; Shirai et al., 2016). Further understanding of the mechanism of metabolic regulation in PCC 6803 is required to guide metabolic engineering research for more efficient production of target compounds (Matsuda et al., 2017). The metabolic regulatory mechanism of photoautotrophic PCC 6803 is unique and distinct from that of heterotrophic bacteria like *Escherichia coli*. Several mechanisms have been reported to play key regulatory roles in PCC 6803. These include a carbon fixation reaction (RuBisCo) as the ultimate rate-limiting step in photosynthetic carbon fixation (Kanno et al., 2017; Raines, 2011; Stitt and Schulze, 1994), a transcriptional global regulation under nitrogen starvation conditions by SigE (Osanai et al., 2005, 2013), a post-translational regulation by CP12 as a response to the redox state (Tamoi et al., 2005; Wedel and Soll, 1998), and allosteric regulation by pyruvate kinase (Pyk) (Knowles et al., 2001). However, our current knowledge on allosteric regulation is still limited, which has become a bottleneck in metabolic engineering studies (Nishiguchi et al., 2019).

Allosteric regulation has been identified and investigated by genetic analysis of over-producing mutants as well as biochemical characterization of metabolic enzymes (Knowles et al., 2001; Takeya et al., 2017, 2018). Furthermore, a more systematic search method consisting of a computer simulation of allosteric regulation using an ensemble of kinetic metabolic models has been recently suggested (Christodoulou et al., 2018). Ensemble modeling of microbial metabolism has been applied to build accurate predictive models by synthesizing the results of multiple models into a single score (Contador et al., 2009; Dash et al., 2017; Khodayari et al., 2014a, 2014b; Khodayari and Maranas, 2016; Rizk and Liao, 2009; Tran et al., 2008). Recent computational simulation of *E. coli* metabolism identified NADPH feedback inhibition on G6PDH, since inhibition has a large contribution to predictability and stability of the kinetic metabolic model of *E. coli* (Christodoulou et al., 2018).

This study aimed to use the ensemble modeling approach to investigate allosteric regulation in the PCC 6803 metabolism. The data driven-computer simulation using metabolic flux, enzyme abundance, and metabolite concentration data successfully identified candidates for allosteric inhibition. The enzyme assay experiment using the recombinant protein confirmed that isocitrate was a non-competitive inhibitor of phosphoribulokinase (Prk) as a novel allosteric regulation of cyanobacteria metabolism.

* Corresponding author. Department of Bioinformatic Engineering, Graduate School of Information Science and Technology, Osaka University, 1-5 Yamadaoka, Suita, Osaka, Japan.
E-mail addresses: hiroki_nishiguchi@bio.eng.osaka-u.ac.jp (H. Nishiguchi), liaoj@gate.sinica.edu.tw (J. Liao), shimizu@ist.osaka-u.ac.jp (H. Shimizu), fmatsuda@ist.osaka-u.ac.jp (F. Matsuda).

https://doi.org/10.1016/j.mec.2020.e00153
Received 4 May 2020; Received in revised form 17 October 2020; Accepted 17 November 2020

Abbreviations

2PG	2-phosphoglycerate
3PG	3-phosphoglycerate
AcCoA	acetyl coenzyme A
aKG	α-ketoglutarate
Cit	citrate
CoA	coenzyme A
DHAP	dihydroxyacetone phosphate
E4P	erythrose 4-phosphate
F6P	fructose 6-phosphate
FBP	fructose 1,6-bisphosphate
G6P	glucose-6-phosphate
G6PDH	glucose-6-phosphate dehydrogenase
GAP	glyceraldehyde 3-phosphate
GAPDH	glyceraldehyde 3-phosphate dehydrogenase
GPM	phosphoglycerate mutase
IsoCIt	isocitrate
NAD(H)	nicotinamide adenine dinucleotide
NADP(H)	nicotinamide adenine dinucleotide phosphate
PEP	phosphoenolpyruvate
PGK	phosphoglycerate kinase
PRK	phosphoribulokinase
PS	photosystem
PYK	pyruvate kinase
Pyr	pyruvate
R5P	ribose 5-phosphate
Ru5P	ribulose 5-phosphate
RuBP	ribulose 1,5-bisphosphate
RuBisCO	ribulose 1,5-bisphosphate carboxylase/oxygenase
S7P	sedoheptulose 7-phosphate
SBP	sedoheptulose 1,7-bisphosphate
TCA cycle	tricarboxylic acid cycle
Xu5P	xylulose 5-phosphate

2. Materials and methods

2.1. Strains and culture conditions

Synechocystis sp. PCC 6803 glucose-tolerant (GT) strain (PCC 6803) as well as its metabolically engineered ethanol producing strain (Et-g, *glgC*:Km^r, NS1:P_{nblA}-*pdc*-*adhII*-Am) were used in this study (Namakoshi et al., 2016; Yoshikawa et al., 2017). The Et-g strain lacks the *glgC* gene and overexpresses *Zymomonas mobilis*-derived pyruvate decarboxylase (*pdc*) and alcohol dehydrogenase (*adhII*) genes.

For the preculture, cells were cultured in 40 mL modified BG11 medium [2.7 μM EDTA disodium salt, 46 μM H_3BO_3, 20 mM HEPES, 1.6 μM $Na_2MoO_4{\cdot}2H_2O$, 220 μM K_2HPO_4, 300 μM $MgSO_4{\cdot}7H_2O$, 260 μM $CaCl_2$, 9.1 μM $MnCl_2{\cdot}4H_2O$, 0.77 μM $ZnSO_4{\cdot}7H_2O$, 0.32 μM $CuSO_4{\cdot}5H_2O$, 0.17 μM $Co(NO_3)_2{\cdot}6H_2O$, 16 μM $FeCl_2{\cdot}4H_2O$ adjusted to a pH of 7.5 using 1 M KOH] containing 50 mM $NaHCO_3$ (in 200 mL flask). The cells were cultivated at 34 °C with a rotary agitation of 150 rpm under continuous illumination (approximately 100 μmol of photons m^{-2} s^{-1}) with white light-emitting diodes (LC-LED450W, TAITEC Co., Ltd., Japan). Kanamycin (10 μg/mL) and ampicillin (1 μg/mL) were added to the preculture of the Et-g strain, as selection markers of genetically engineered cells. The bacterial cell density was measured as absorbance at 730 nm (OD_{730}) using a spectrophotometer (UVmini-1240, Shimadzu Co.). The OD_{730} was converted to a dry cell weight using the following formula: dry cell weight (g dry cell weight [DCW] l^{-1}) = $OD_{730} \times 0.16$ (g DCW l^{-1} OD_{730}^{-1}).

For the ethanol production test, cells were inoculated in 4 mL BG11 medium containing 50 mM $NaHCO_3$ (in 20 mL test tube) with an initial OD_{730} of 1.0. The cells were cultured for 4 days under the same conditions. Every 24 h, 400 μL of culture broth was collected for the medium component analysis, which was complemented by the addition of 400 μL of BG11 containing 500 mM $NaHCO_3$. No antibiotics were added to the culture of the Et-g strain. Extracellular ethanol concentration was analyzed by gas chromatography (GC; Agilent 7890 A GC [Agilent]), using a Restek 10,657 Stabiliwax column (60 m × 0.32 mm ID × 1 μm, Shimadzu). The column temperature was 70 °C, the injector temperature was 250 °C, and an FID was used for detection.

For the metabolome and proteome analysis, cells were inoculated in 40 mL BG11 medium containing 50 mM $NaHCO_3$ (in 100 mL flask) with an initial OD_{730} of 0.05 and cultured for 48 h under the same conditions. No antibiotics were added to the culture of the Et-g strain.

2.2. Metabolome and proteome analysis

Cells were collected 48 h after the start of cultivation. Cells in the culture broth (20 mL) were filtered through a 0.5-μm pore size filter (PTFE-type membrane, Advantec, Japan), immediately immersed in 1.6 mL methanol (−80 °C), and then stored at −80 °C until extraction. Intracellular metabolites were extracted by the water-methanol-chloroform method using a previously described method (Nishino et al., 2015). The metabolite extracts were employed in the targeted metabolome analyses using liquid-chromatography (LC)/mass spectrometry (MS) as described previously (Nishino et al., 2015). For the analysis of organic acids, metabolites were derivatized using methoxyamine hydrochloride in pyridine and *N*-methyl-*N*-(trimethylsilyl) trifluoroacetamide, and then analyzed by GC–MS, as described previously (GCMS QP-2010 system, Shimadzu, Kyoto, Japan) (Nagai et al., 2018).

Targeted proteome analysis was performed using a previously described method (Tokumaru et al., 2018). Briefly, crude proteins were extracted from PCC 6803 cells and digested with trypsin. Equal amounts of digested peptides derived from the target strains (cultured using non-labeled glucose) and isotope-labeled strains (cultured in ^{15}N medium as an internal standard) were mixed. The peptide samples (2 μL) were analyzed by a previously described method using a nano-LCMS system (LC-20ADnano and LCMS-8040, Shimadzu, Kyoto, Japan) (Tokumaru et al., 2018). The MRM assay method for targeted proteome analysis was obtained from a previous study (Tokumaru et al., 2018). Chromatographic data were processed using Skyline software, version 3.1 (Bereman et al., 2012) to determine relative peak areas for all peptides using ^{15}N labeled peptides as internal standards.

2.3. Preparation of kinetic model

The metabolic model of the PCC 6803 strain constructed in the previous study was used with slight modifications (Supplementary Table 1, 2 and 3) (Nishiguchi et al., 2019). The reaction rate equation for pyruvate kinase was changed to the irreversible Michaelis-Menten equation for the bi-bi reaction (Supplementary Table 3). Furthermore, the ethanol biosynthesis pathway was added as a reaction with constant metabolic flow. The metabolic model used in this study includes 34 metabolic reactions, 6 photosynthetic reactions, 3 buffer reactions, and 4 reactions pertaining to biomass synthesis, glycogen degradation, and ethanol production. The model consisted of 42 metabolites, 109 K_M values, and 31 *Keq* parameters (Supplementary Table 4). For the photosynthetic reactions, ATP synthase was described using the irreversible Michaelis–Menten equation, and the other 5 reactions were described by the mass action equation. Metabolic-flux levels of biomass synthesis, glycogen degradation, and glucose uptake were set at constant levels based on their respective measured values (Supplementary Table 1). Generalized Michaelis–Menten equations were employed for other reactions, as well as for reactions with allosteric inhibition (Supplementary

Table 3) (Liebermeister et al., 2010). The coefficients of each metabolite used for biomass synthesis were calculated based on literature data (Shastri and Morgan, 2005).

2.4. Preparation of the trans-omics dataset

The trans-omics dataset of PCC 6803 cells grown under photoautotrophic and mixotrophic conditions was obtained from our previous studies (Nakajima et al., 2014, 2017). Missing values in the metabolome and proteome data were imputed using the following method: the concentrations of eight metabolites were arbitrarily set to 0.01 μmol (g DCW)$^{-1}$ (BPG, SBP, glyoxylate, OAA, Q, QH2, Hex, Photon, SubsGlc, CO_2, glycogen) (Supplementary Table 2); the G3P concentration was theoretically calculated as the reaction catalyzed by triosephosphate isomerase (dihydroxyacetone phosphate <-> glyceraldehyde 3-phophate) in a near-equilibrium reaction state; units of all data and parameters were adjusted to μmol (g DCW)$^{-1}$; the expression levels of unmeasured proteins were considered constant. The specific volume of cyanobacteria (2.66 mLg dry cell weight) was used in this study (Lawrence et al., 1998; Loferer-Krossbacher et al., 1998).

2.5. Ensemble modeling

In silico modeling experiments were performed using an in-house script written with Python 3.6, NumPy 1.16, and Scipy 0.17. For the numerical integration of the metabolic model, the scipy. integrate.odeint was used as an ordinary differential-equation solver. The convergence of the models was checked by comparison of all metabolite concentration levels between current and previous steps ($\Delta < 0.00001$), and confirmed by performing linear-stability analysis. The K_M and K_{eq} values were randomly sampled from a log uniform distribution (Supplementary Table 4). Because the measured and predicted values were available from the literature and the eQuilibrator database (Flamholz et al., 2012), 7 K_M values for PRK, PGK, and RuBisCo and all K_{eq} values were randomly sampled at 1/5 to 5 times the measured values (Tsukamoto et al., 2013). Other K_M and K_i values were randomly sampled from a uniform distribution between 0.01 and 100, with a logarithmic scale. (Supplementary Table 4). All ppi values were randomly sampled from a uniform distribution between 0.0 and 1.0 (Supplementary Table 4).

2.6. Expression of recombinant protein

The *prk* and *gpm* genes were amplified by PCR with KOD FX Neo (Toyobo Co., Ltd., Osaka, Japan) from the genomic DNA of PCC 6803 using the following primers (prk/forward cgGAATTCATGACCACACAGCTAGACCG, prk/reverse gCTCGAGTTACACAGAGGCCGGGACCT, gpm/forward cgGGATCCATGGCAGAGGCACCGATCGC, gpm/reverse cgCTCGAGCTAACGGGAGAGATTGACCG). Each amplified fragment was cloned into a Zero Blunt TOPO vector (Thermo Fisher Scientific, Waltham, MA), followed by sequence confirmation. The *Eco*RI - *Xho*I fragments (for *prk*) and *Bam*HI - *Xho*I fragments (for *gpm*) of Zero Blunt TOPO were cloned into the same restriction site of the pET28-a(+) vector, generating pET28-a(+)*/prk*, and pET28-a(+)*/gpm*. The recombinant strains of BL21(DE3) harboring the plasmids were cultured overnight in LB medium at 37 °C. The culture broths were transferred to 200 mL baffled Erlenmeyer flasks containing fresh 50 mL LB medium (initial OD = 0.05) and cultured at 30 °C in a rotary shaking incubator at 200 rpm (BR-43FL, Taitec Tokyo, Japan). Isopropyl-β-*d*-thiogalactopyranoside was added at OD = 0.5 (final conc. 0.1 mM). After 20 h of cultivation, the cell pellets were obtained from 10 mL of culture broth by centrifugation at 2500×*g* for 5 min at 4 °C and lyophilized using a xTractorTM Buffer kit (TaKaRa, Kyoto, Japan). Target proteins were purified using Capturem His-Tagged Purification Miniprep kit (TaKaRa) and Centrifugal Filter Units (30 K, Millipore, Burlington, MA) to replace with 1 M HEPES buffer (pH 7.5). Purification was confirmed by SDS-PAGE using e-PAGEL HR (ATTO) with CBB staining. Protein concentration was determined using a Pierce BCA Protein Assay Kit (Thermo).

2.7. Enzymatic assay of Prk and Gpm

The enzyme activity of the purified Prk was assayed by a coupling reaction catalyzed by pyruvate kinase and lactate dehydrogenase at 37 °C as previously described (Wadano et al., 1998). Gpm activity was measured by a coupling reaction catalyzed by enolase, pyruvate kinase, and lactate dehydrogenase. The reaction mixture contained 40 mM Tris-HCl (pH 7.9), 5 mM KCl, 0.6 mM MgSO4, 0.054 mM PEP, 0.036 mM EDTA, 100 μM NADH, 3.3 mM glutathione, and approximately 10 U/mL of pyruvate kinase and lactate dehydrogenase (from Rabbit P0294 Sigma–Aldrich Co, St. Louis, MI)) was commonly used. For Gpm, 1.2 mM ADP and 458 unit/mL enolase (Sigma–Aldrich E6126) was added to the mixture. The decrease in absorbance of NADH at 340 nm was monitored for 20 min using a microtiter plate reader (SYNERGY, BioTec, Green Mountains, VT). Enzyme activity was determined from ΔA_{340nm} and the extinction coefficient of NADH (6300 L mol^{-1} cm^{-1}).

3. Results

3.1. Design of in silico simulations

In this study, trans-omics data-driven ensemble modeling was performed using three datasets obtained from the PCC 6803 GT strain under photoautotrophic conditions (auto), a metabolically engineered strain (Et-g) under photoautotrophic conditions (EtOH), and the GT strain under mixotrophic conditions (mixo). Computer simulations were used to predict allosteric inhibition (or a combination of an inhibitor metabolite and a regulated enzyme) effectively working in the PCC 6803 metabolism under these conditions. Two *in silico* simulations (Simulations I and II, Table 1) were performed for this purpose by the procedure shown in Figs. 1 and 2. Simulation I was for the systematic survey of allosteric inhibition using the auto and EtOH datasets. Simulation II was for validation of the systematic search result using different (auto and mixo) datasets (Table 1).

4. Detailed procedures were shown in Figs. 1 and 2

Figs. 1 and 2 show the procedures for the *in silico* simulation. For explanatory purposes, a metabolic network including three reactions was used in Figs. 1 and 2. The *in silico* simulations required two trans-omics datasets obtained from two distinct conditions (designated as conditions X and Y as an example, Fig. 1A). One dataset included metabolome ([*S*]), fluxome (*J*), and proteome data ([*E*]). Fluxome (*J*) data of condition Y was not used in this study.

Here, "structure of metabolic model" indicated a collection metabolic reactions (the stoichiometry and rate equation) including allosteric inhibitions. The values of all parameters (i.e., Michaelis (K_M) and reaction rate (k) constant) were undetermined. "Plain structure" meant a structure without allosteric inhibition (Fig. 1B).

It should be noted that an "ensemble of models" indicated a population of metabolic models with an identical structure but different parameter sets in this study. All models in an ensemble were generated using an identical plain structure, and then equally modified by an addition of same allosteric inhibition, as mentioned below. Thus, an ensemble of models, including various structures, was not used in this study.

An ensemble of models was prepared from the plain structure (Fig. 1C). Following the assignment of [*E*], [*S*], and *J* levels of condition X dataset, each parameter in three rate equations such as the Michaelis constant (K_M) were randomly determined. For the case of the irreversible Michaelis–Menten equation, $J = k[E][S]/([S] + K_M)$, K_M was obtained by random sampling. The remaining constant k was determined by $k = J([S] + K_M)/[E][S]$, using the [*E*], [*S*], and *J* levels available from the dataset. By the procedure, a metabolic model with the plain structure (no

Table 1
Comparison of two *in silico* simulations (Simulations I and II) to predict allosteric inhibition effectively working in the PCC 6803 metabolism.

Procedures[1)]	Simulation I: Systematic search of allosteric regulation using trans-omics data	Simulation II: Validation of systematic search using different datasets
Trans-omics dataset (Condition X)	*Synechocystis* sp. PCC 6803 GT strain under photoautotrophic condition (auto). Metabolome: $[S]_{auto}$ (Nishiguchi et al., 2019). Fluxome: J_{auto} (Nakajima et al., 2017). Proteome: $[E]_{auto}$ (Nishiguchi et al., 2019)	Same as on the left
Trans-omics dataset (Condition Y)	Metabolically engineered Et-g strain producing ethanol under the photoautotrophic condition (EtOH). Metabolome: $[S]_{EtOH}$ (This study). Proteome: $[E]_{EtOH}$ (This study)	Mixotrophic condition (mixo). Metabolome: $[S]_{mixo}$ (Yoshikawa et al., 2013). Proteome: $[E]_{mixo}$ (Nishiguchi et al., 2019)
Plain structure of metabolic model	Total 47 reactions, including 34 metabolic reactions, 6 photosynthetic reactions, 3 buffer reactions, and 4 reactions responsible for biomass synthesis, glycogen degradation, and ethanol production without allosteric regulations.	Same as on the left
Preparation of an ensemble of models	By the method 1 (Fig. 1C). Ensemble of 10,000 models reproducing the auto condition (no allosteric regulation, distinct random parameter sets)	By the method 2 (Fig. 1D). Ensemble of 100,000 models reproducing the auto condition (no allosteric regulation, distinct random parameter sets)
Systematic survey of allosteric inhibition	Total 1056 combinations (single allosteric inhibition among 32 metabolites by 33 enzymes).	Total 84 combinations (single allosteric inhibition among 14 top-ranked inhibitor metabolites and the six top-ranked enzymes in Simulation I)
Scoring method	Median of sum of square (RSS) for remaining models	Survival rate in a numerical integration

allosteric regulation, random parameters) reproducing condition X was obtained. To select better models, the model was checked by using condition Y dataset. After the levels of [*E*] of condition Y were assigned for all reactions, a new steady state was found by numerical integration. A surviving model without divergence was added to an ensemble of models. By iteration of the procedure, an ensemble of models with the identical plain structure (no allosteric regulation, distinct random parameter sets) reproducing condition X was generated (Fig. 1C). The method 1 was used for Simulation I (Table 1). For the case of low survival rate during the numerical integration such as Simulation II, an ensemble of models was produced without checking (The method 2, Fig. 1D).

Fig. 2 shows a procedure for a test of an allosteric inhibition using the ensemble of models. An allosteric inhibition seemed to be working in the PCC 6803 if an addition of the allosteric inhibition can improve a prediction capability and robustness against metabolic perturbations of the ensemble. To test an allosteric inhibition, same one allosteric inhibition was added to the structure of all models in the ensemble (Fig. 2A). Thus, an ensemble of models with an identical modified structure with different parameter sets was used to test the allosteric regulation. Structures with two or more allosteric inhibitions were not considered in this study. Fig. 2 shows the addition of allosteric inhibition of the enzyme (E_A) by the inhibitor metabolite (S_3) as an example. The addition of allosteric inhibition was performed by replacement with a rate equation including allosteric inhibition. For the irreversible Michaelis–Menten equation, the rate equation including allosteric inhibition was: $J = (\text{ppi} + (1\text{-ppi})\ K_i/(K_i + [I]))\ k[E][S]/([S] + K_M)$, where $[I]$ and K_i are the concentration of inhibitor and the inhibition constant, respectively. Partial inhibition by inhibitor binding (range: 0–1.0) is represented by the parameter ppi. For the replaced rate equation, the random sampling of K_{eq}, K_M, K_i, and ppi, as well as the determination of *k* using trans-omics data ([*E*], [*S*], and *J*) were performed (Fig. 2A).

To test the added allosteric inhibition (Fig. 2B), following the protein abundances of all reactions were changed to the [*E*] levels of condition Y, new steady states were found by numerical integration. Some of the models were discarded due to divergence. Finally, an ensemble of the remaining models reached new steady states was obtained. The simulation result was scored by two methods (Fig. 2C). The first was the survival rate in the numerical integration to assess the robustness of the modified structure. The second method was the similarity (residual sum of square, $RSS = \Sigma([S]_{pred} - [S])^2$) between the predicted ($[S]_{pred}$) and the measured ([*S*]) metabolite abundances under condition Y. A median RSS of multiple remaining models were used as a score of the predictability (Fig. 2C). The procedure was performed for all allosteric inhibitions tested. Scores of all tests were compared to find promising allosteric inhibitions.

4.1. Preparation of trans-omics dataset

The auto dataset, including $[E]_{auto}$, $[S]_{auto}$, and J_{auto}, as well as the mixo dataset, including $[E]_{mixo}$, and $[S]_{mixo}$, were obtained from literatures (Nakajima et al., 2014, 2017; Nishiguchi et al., 2019; Yoshikawa et al., 2013). (Table 1, Supplementary Tables 1 and 2). It is worth noting that the metabolic flux levels of J_{auto} during the exponential growth phase (OD_{730} ~1.0), were prepared by combining the ^{13}C-based metabolic flux analyses (Nakajima et al., 2017) with the flux balance analysis (FBA) performed in our previous study (Nishiguchi et al., 2019). Carbon flux levels were determined based on the ^{13}C-based metabolic flux analyses (Nakajima et al., 2014, 2017). In the metabolic flux data, the metabolic flux level of malic enzyme (0.14 mmol (g dry cell weight)$^{-1}$ h^{-1}) was lower than that of pyruvate kinase (0.6 mmol (g dry cell weight)$^{-1}$ h^{-1}) (Supplementary Table 1). Conversely, malic enzyme has previously been reported as a major pyruvate source in *Synechococcus elongatus* PCC 7942, as pyruvate kinase was inhibited under photosynthetic conditions (Jazmin et al., 2017; Young et al., 2011). Since the ^{13}C-based metabolic flux analyses did not consider the photosystem, FBA was performed to estimate flux levels of the photosystem reactions by minimizing the photon flux as the objective function (Nishiguchi et al., 2019). The photosystem reactions included photosystems 1 and 2 (PS1 and PS2), ATP synthase, cytochrome oxidase, and the cyclic electron flow (Supplementary Table 1). Other mechanisms, like the water-water cycle, were not considered.

4.2. Acquisition of proteome and metabolome data from metabolically engineered PCC 6803 strain producing ethanol for modeling

The EtOH dataset, including $[E]_{EtOH}$ and $[S]_{EtOH}$, was obtained from the ethanol-producing PCC 6803 (Et-g) strain in this study The Et-g strain was constructed by over-expressing pyruvate decarboxylase (*pdc*) and alcohol dehydrogenase (*adh*II) genes from *Zymomonas mobilis* and deleting *the glgX* gene responsible for the glycogen biosynthetic pathway (Namakoshi et al., 2016). Batch cultures of WT and Et-g strains were performed under photoautotrophic conditions. The culture profile data showed that the Et-g strain continued cell growth and ethanol production for 96 h (Supplementary Fig. 1). The specific production rate of ethanol was determined to be 5.2 ± 0.0 mg g-DCW^{-1} h^{-1} that was similar to the literature value. The specific cell growth rate of the Et-g strains (0.013 ± 0.000 h^{-1}) was 19% lower than that of the wild type strains (0.016 ± 0.000 h^{-1}), probably due to the stress derived from ethanol production by the artificial pathway. Cyanobacteria or PCC 6803 strains lacking glycogen biosynthesis pathway produce organic acids under nitrogen starvation conditions (Carrieri et al., 2017). However, GC-MS analysis of the culture medium of this study showed that no other metabolites were produced during the culture period (data not shown).

Cells of WT and Et-g strains were collected at a mid-log phase (at 48

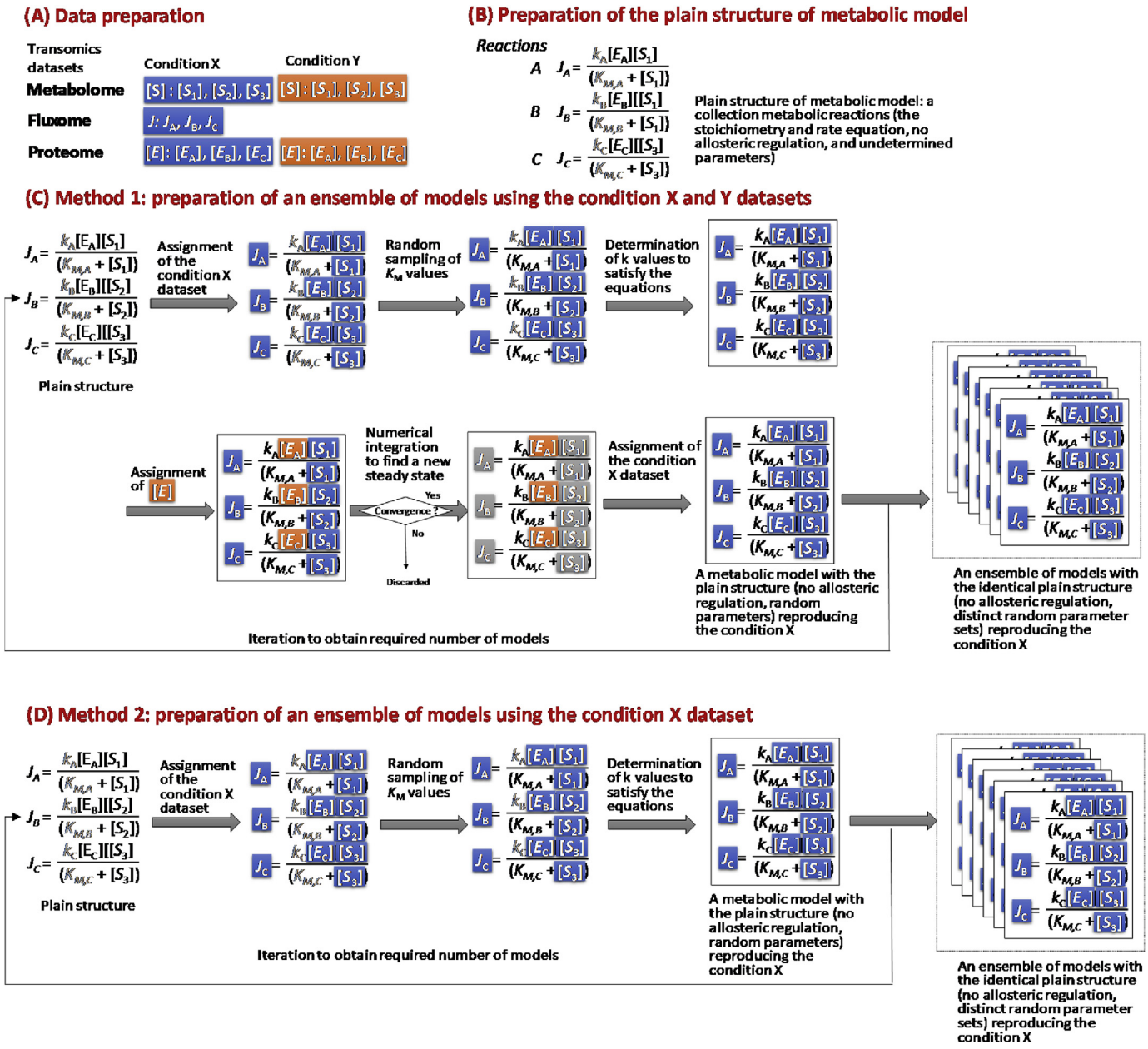

Fig. 1. The procedures for preparation of an ensemble of models. The figure describes required (A) trans-omics datasets, (B) the plain structure of metabolic model, and (C and D) procedures for preparation of an ensemble of models by method 1 and 2. For explanatory purposes, a metabolic network including three reactions was used. Gray characters indicate parameters whose values were undetermined. Colors of boxes represent measured trans-omics data obtained at conditions X (blue) and Y (orange) and predicted values obtained by numerical integration (gray).

h) and their metabolic profiles were measured by targeted metabolome analyses (Fig. 3 and Supplementary Table 5). The comparison of the relative metabolite abundance showed that the amounts of metabolites in the lower glycolysis, such as 3-phosphoglycerate (3PG), increased in the Et-g strain, (3.6 times). On the contrary, the amounts of G6P and F6P drastically decreased, suggesting that carbon supply in glycogen biosynthesis was suppressed in the Et-g strain. The amount of metabolites at the entry point of the TCA cycle, such as citrate and isocitrate, slightly decreased in the Et-g strains. PCC 6803 is known to have a redox regulation by which low NADP(H)/NAD(H) level induces the formation of a GAPDH-CP12-PRK super complex to suppress the metabolic activity of the Calvin-cycle (Tamoi et al., 2005). The suppression of the Calvin cycle would not work in the Et-g strains since the NADP(H)/NAD(H) level in the Et-g strain was larger than that of the WT, as shown in Fig. 3.

Moreover, relative abundances of central metabolism-related enzymes as well as the photosystem-related proteins (60 proteins in total) were successfully measured by targeted proteomics (Supplementary Table 6). The results showed that the abundance of most proteins decreased in the Et-g strain. The abundances of PsaA and GabD in the Et-g strain were 0.25 and 0.33 times relative to that of the WT, respectively. The key enzymes involved in carbon fixation, including Prk, RbcL, RbcS, and Pgk, were also down-regulated.

4.3. Preparation of plain structure of metabolic model

Rate equations for 47 reactions of the PCC 6803 metabolic network, without allosteric regulations, were prepared as the "plain structure" of the metabolic model (Supplementary Table 1). The plain structure was prepared based on a metabolic network used in ensemble modeling in our previous study, which was able to successfully identify metabolic

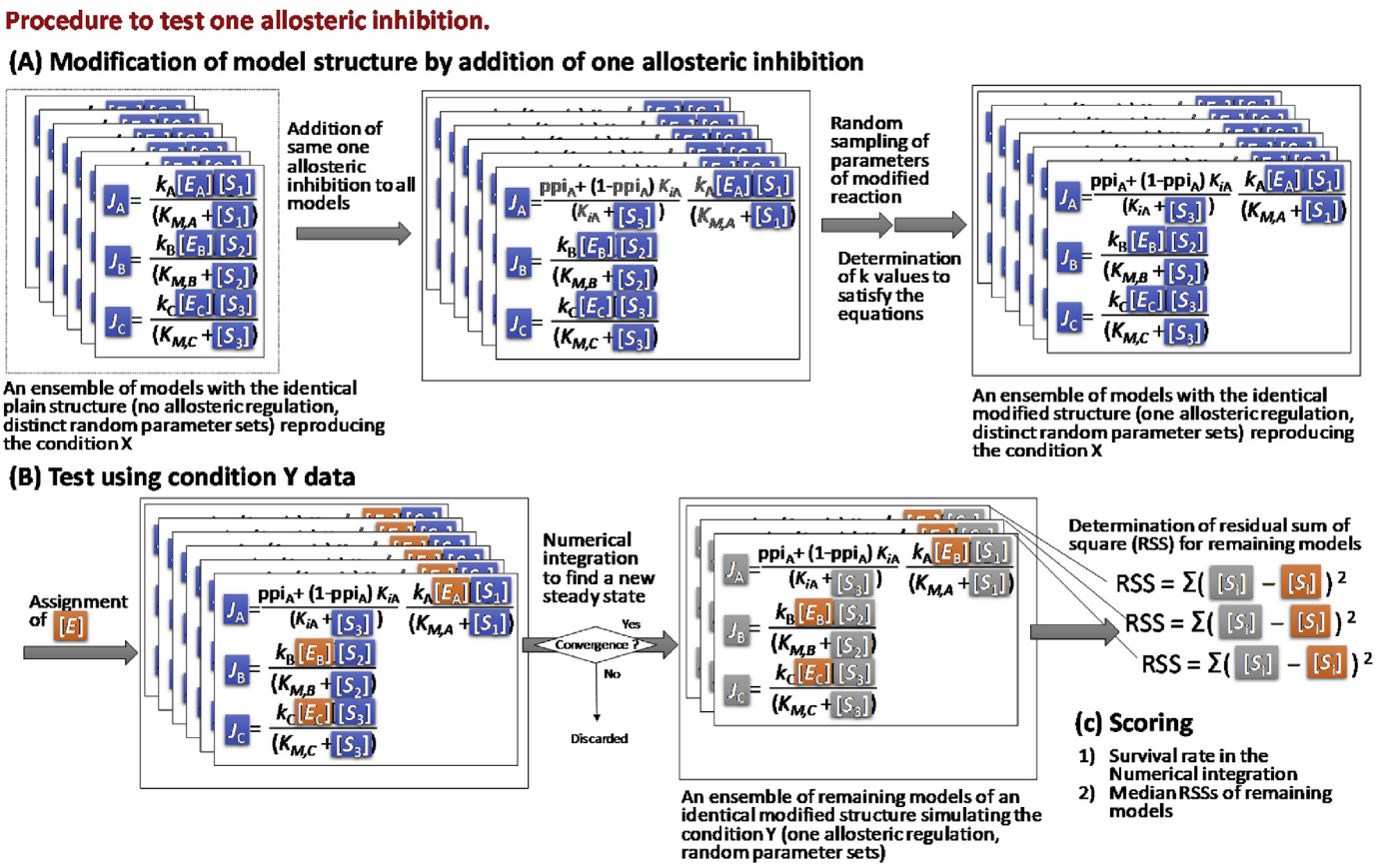

Fig. 2. The procedure to test one allosteric regulation. For explanatory purposes, a metabolic network including three reactions and their modification by addition of allosteric inhibition of enzyme $[E_A]$ by metabolite $[S_3]$ was represented. Gray characters indicate parameters whose values were undetermined. Colors of boxes represent measured trans-omics data obtained at conditions X (blue) and Y (orange) and predicted values obtained by numerical integration (gray). The procedure was performed for all tested allosteric inhibitions.

engineering targets (Nishiguchi et al., 2019). The plain structure included 34 metabolic reactions, 6 photosynthetic reactions, 3 buffer reactions, and 4 reactions responsible for biomass synthesis, glycogen degradation, and ethanol production, respectively. This network of 34 metabolic reactions is shown in Fig. 3. The TCA cycle was reported to operate as a complete cycle under photoautotrophic conditions. However, the metabolic pathway from aKG to succinate is bifurcated (Knoop et al., 2013). In this study, bifurcated pathways were considered as a single reaction (GabD) for the sake of simplification. The reaction kinetics of the enzyme and five photosystem reactions were described using generalized Michaelis–Menten and mass action equations (Supplementary Table 3). The plain structure did not include allosteric inhibition and no fixed parameter values (Fig. 1B).

4.4. Simulation I: systematic search of allosteric regulation using trans-omics data

Simulation I was performed using the auto and EtOH datasets (Table 1). An ensemble of 10,000 models with the identical plain structure (no allosteric regulation, distinct random parameter sets) reproducing condition X was prepared by the method 1 (Fig. 1C). It should be noted that, for random sampling of parameters, K_M and K_I was obtained from a log uniform distribution (10^{-2}–10^{2} μmol (g-DCW)$^{-1}$) (Supplementary Table 4). For reversible reactions, K_{eq} was also included in the rate equations. In the cases of K_{eq} values as well as K_M values for phosphoribulokinase (PRK), phosphoglycerate kinase (PGK), and RuBisCo, the lower and upper limits (20%–500%) of known values from the database, or literature, were used (Tsukamoto et al., 2013). Moreover, unstable or unpromising models were removed by linear stability analysis to reduce the number of models served for the computationally expensive numerical integration step. The procedure was repeated until 10,000 models were obtained (approximately 4 h of parallel calculations using an Intel Core i7 processor).

Using the ensemble of 10,000 models and the mixo dataset, the role of allosteric inhibition was tested for 1056 combinations (allosteric inhibition among 32 metabolites by 33 enzymes) by the procedure shown in Fig. 2. The systematic survey of 1056 cases could be completed within approximate 7 days. Here, the median RSS was used for scoring, as it is a reliable value that can be obtained from the large numbers of remaining models. As a control, the median RSS of the ensemble of the models without allosteric inhibition was determined to be 1054 (Table 2). Among the 1056 allosteric regulations tested, a total of 239 cases showed smaller median RSSs than that of the control (Supplementary Table 7). Smaller median RSS values suggested that these allosteric inhibitions would be effective in improving the predictability of the ensemble.

The top 10 allosteric inhibitions, with the smallest median RSS among the 1056 cases, are listed in Table 2 (all results in Supplementary Table 7). The results showed that intermediates around the entrance of the TCA cycle, including acetyl-Coenzyme A (AcCoA), citrate, isocitrate, and α-ketoglutarate (aKG), would be effective inhibitors of pyruvate kinase (Pyk), phosphoribulokinase (Prk), and phosphoglycerate mutase (Gpm). For example, when the allosteric inhibition of Pyk protein by aKG was added to all 10,000 models in the ensemble, which was followed by numerical integrations, a total of 6897 models were found reaching a new stable steady state without divergence (survival rate = 69.0%), with a median RSS of 951 (Rank 1 in Table 2, Supplementary Table S7). For the allosteric inhibition of Prk protein by isocitrate, the median RSS of the 6980 remaining models (survival rate = 69.8%) was 959 (Rank 5 in

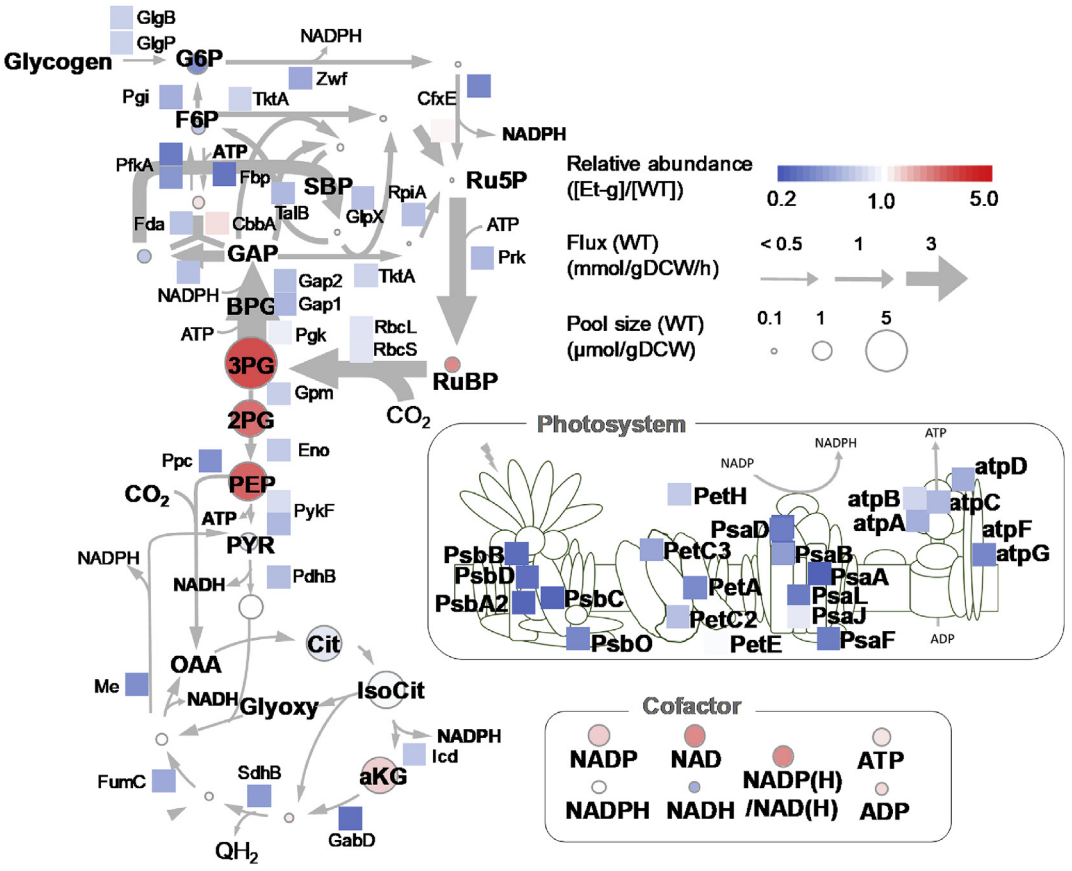

Fig. 3. Metabolic network of *Synechocystis* sp. PCC 6803 strain. The trans-omics dataset, including the metabolite concentration, protein abundance, and metabolic flux levels used in this study is represented. The metabolic model consisted of 47 reaction rate equations. The circle areas and arrow widths are proportional to the literature reported metabolite concentration ($[S]_{auto}$) and flux (J_{auto}) levels of the wild-type strain under the photoautotrophic condition (auto), respectively. Boxes with protein names indicate proteins whose relative abundances ($[E]_{EtOH}/[E]_{auto}$) in the Et-g strain under the photoautotrophic condition (EtOH) were determined by targeted proteome analysis in this study. The colors of circles and boxes represent a heatmap representation of the relative abundance levels (EtOH:auto ratio). Metabolite concentrations and protein abundances were determined by analyzing samples in triplicates.

Table 2, Supplementary Table S7).

4.5. Simulation II: validation of systematic search using different datasets

Results of Simulation I were validated by similar computer simulations using the different datasets (Simulation II, Table 1). The mixo dataset obtained from the GT strain under mixotrophic conditions (mixo) was used in addition to the auto dataset (Nishiguchi et al., 2019; Yoshikawa et al., 2013). It is known that when the medium is supplemented with glucose under conditions with light, the PCC 6803 strain can use glucose as an additional carbon source (Yoshikawa et al., 2013). A previous study demonstrated that the dataset was effective in constructing predictable kinetic models of PCC 6803 (Nishiguchi et al., 2019).

Ensemble of 100,000 models reproducing the auto condition (no allosteric regulation, distinct random parameter sets) was produced using the method 2 (Fig. 1D). The method 2 was used because the survival rate of the numerical integration using the mixo data was too low to gather enough number of models.

Allosteric inhibitions were tested for 84 combinations of the 14 top-ranked inhibitor metabolites and the six top-ranked enzymes. As a control, the procedure was performed without the addition of allosteric inhibition. The survival rates after three trials were 8, 10, and 12 among 100,000 models, with median RSSs of 438, 478, and 623, respectively (Table 2). The low survival rate (approximately 0.01%) was due to large fluctuations in enzyme abundance between $[E]_{mixo}$ and $[E]_{auto}$. Since the median RSS values were unstable for small numbers of models, the number of surviving models was employed for scoring.

Computer simulation results are shown in Table 2 (all results in Supplementary Table 8). The total calculation time was approximately 12 days. Results showed that the top 7 candidates from the previous section using the EtOH dataset, were also ranked within the top 10. For example, the survival rate increased to 59/100,000 after the allosteric inhibition of Pyk protein by aKG was added to all models in the ensemble (Rank 7, median RSS = 516 (data not shown)). The survival rate was 65/100,000 for the case of the allosteric inhibition of Prk protein by isocitrate (Rank 5, median RSS = 402). These results suggested that certain allosteric inhibitions could contribute to the stability of the kinetic metabolic model of PCC 6803.

4.6. Enzyme assay of predicted allosteric regulations

Two computer simulation results were compared to find plausible allosteric inhibitions (Table 2). The results showed that only three regulated enzymes (Pyk, Prk, and Gpm) and five inhibitor metabolites (aKG, isocitrate, AcCoA, citrate, Pyr) were included in the list. Among them, the inhibition of Pyk by aKG, isocitrate, AcCoA, citrate, and Pyr is listed in Table 2. Indeed, the inhibition of Pyk by aKG and citrate was previously reported in the biochemical characterization of Pyk from *Synechococcus* PCC 6301 (Knowles et al., 2001). In this report, malate, FBP, and ATP were also found to inhibit Pyk from *Synechococcus* PCC 6301. The rankings of Pyk inhibition by malate FBP, and ATP, in the systematic survey, were 56, 40, and 42 out of 1056 cases, respectively (Supplementary Table 7). Although a detailed investigation of PCC 6803 enzymes is still needed, the computer simulation could address known

Table 2
Systematic search of allosteric inhibition using trans-omics data by Simulation I and Simulation II.

Rank	Enzyme	Inhibitor	Number of survived model	Median Residual Sum of Square	Experimental assessment
Simulation I (using Ensemble of 10,000 models)					
1	Pyk	aKG	6897	951	24% inhibition by 5 mM (Knowles et al., 2001)
2	Pyk	isocitrate	6964	955	No
3	Prk	aKG	6962	956	No
4	Pyk	citrate	7009	958	41% inhibition by 5 mM (Knowles et al., 2001)
5	Prk	isocitrate	6980	959	K_i = 1.45 mM (This study)
6	Prk	citrate	7047	961	No
7	Pyk	AcCoA	7940	979	No
8	Gpm	aKG	7390	982	No inhibition at 1.0 mM (This study)
9	Prk	AcCoA	7318	983	No
10	Gpm	isocitrate	7473	983	No
Control	No allosteric inhibition		10,000	1054	No
Simulation II (using Ensemble of 100,000 models)					
1	Prk	Pyr	277	Nd	No
2	Pyk	Pyr	74	Nd	No
3	Prk	AcCoA	73	Nd	No
4	Pyk	AcCoA	70	Nd	No
5	Prk	isocitrate	65	402	K_i = 1.45 mM (This study)
6	Prk	citrate	60	Nd	No
7	Pyk	aKG	59	516	24% inhibition by 5 mM (Knowles et al., 2001)
8	Pyk	isocitrate	55	Nd	No
9	Pyk	citrate	54	Nd	41% inhibition by 5 mM (Knowles et al., 2001)
10	Prk	aKG	53	Nd	No
Control	No allosteric inhibition		8–11	Nd	Control

allosteric inhibitions of Pyk (Knowles et al., 2001).

On the other hand, as far as we have investigated, allosteric inhibitions for Prk and Gpm in Table 1 have not been reported in cyanobacteria. Since the inhibition of Prk by isocitrate ranked 5th the results of Simulation I and II, respectively, this combination was selected as a candidate for the biochemical assay. Moreover, we selected an inhibition of aKG to Gpm as an additional candidate since it has been reported that the modification of Gpm expression level could affect the carbon flow level from 3 PG to Pyr (Oliver and Atsumi, 2015).

The predicted allosteric regulations were tested by *in vitro* enzyme assays using recombinant Prk and Gpm proteins. Open reading frames of *prk* and *gpm* genes were cloned from the PCC 6803 genome and then used for the construction of *E. coli* expressing the recombinant proteins (Supplementary Fig. 2). Enzyme assay using the purified recombinant Prk showed that K_M for Ru5P was 0.48 mM. This value was similar to that of Prk from *Synechococcus* PCC 7942 (0.27 mM, Supplementary Fig. 3) (Wadano et al., 1998). Furthermore, the K_M value of Gpm for 3 PG was 0.23 mM. The result implied that the reaction rate of Prk could be sensitive to Ru5P concentration because the measured concentration of Ru5P in PCC 6803 under photoautotrophic conditions (0.005 mM) was far below the K_M value. In contrast, the intracellular 3 PG concentration (2.7 mM) was much larger than the K_M value, indicating that the reaction rate of Gpm was likely to be insensitive to the substrate concentration.

Next, the effects of isocitrate on Prk activity was tested by the enzyme assay. The concentrations of isocitrate were set at similar levels to their intracellular concentrations under photoautotrophic conditions. The results showed that isocitrate inhibited the reaction rate of Prk by approximately 50% (Fig. 4a). The enzyme assay also showed that no inhibition was observed for Gpm upon addition of aKG. The Dixon plot analysis revealed that inhibition by isocitrate occurred in a noncompetitive manner and the inhibition constant (*Ki*) was deduced to be 1.45 ± 0.13 mM (Fig. 4b). Since the *Ki* value was similar to the intracellular concentration of isocitrate (1.4 mM), Prk was allosterically inhibited by isocitrate under photoautotrophic conditions (Fig. 4c).

5. Discussion

This study examined the application of a computer simulation of metabolism for the systematic search of allosteric regulation in photosynthetic bacteria. The trans-omics data-driven ensemble kinetic model was employed for the simulation of allosteric regulations in PCC 6803 (Figs. 1 and 2 and Table 1). The computer simulation successfully identified several candidates contributing to the reproducibility and stability of the kinetic model of PCC 6803 metabolism (Table 2). One of the candidates (inhibition of Pyr by citrate) was in agreement with literature reported allosteric regulation (Knowles et al., 2001). Moreover, the inhibition of Prk by isocitrate was confirmed as a novel allosteric regulator in cyanobacteria by enzyme assay using the recombinant protein (Fig. 4). These results support that the computer simulation-based method is effective for the systematic search of allosteric regulation. This study demonstrated that in addition to the short time series data of metabolite concentration after perturbation (Christodoulou et al., 2018), datasets obtained from two distinct stationary states were also available for systematic searching using protein abundance data. However, the ensemble modeling approach was conducted by sparse sampling from a large parameter space. Although the ensembles of models as large as possible were used in this study, computer simulations using more calculations are preferable for more a detailed investigation of the metabolic systems.

The list shown in Table 2 did not address some known allosteric regulation in cyanobacteria. For instance, biochemical characterization reported that 6 PG inhibited Prk (116th in the systematic survey, Supplementary Table 7), RuBP inhibited RuBisCo (537th) in *Synechococcus elongatus* PCC 7942, and malate inhibited phosphoenolpyruvate carboxylase in *Synechocystis* sp. PCC 6803 (688th), respectively (Lee et al., 1991; Spreitzer and Salvucci, 2002; Takeya et al., 2017; Wadano et al., 1998). The probable reason for this is that the allosteric regulations were not working in the simulated condition of PCC 6803 because the computer simulation method depended on the dataset used for the systematic searching. It was expected that other allosteric regulations would be found by the computer simulation method by using other trans-omics datasets obtained from distinct metabolic states.

This study experimentally identified isocitrate as a novel allosteric inhibitor of Prk in cyanobacteria (Fig. 4), although a more detailed biochemical characterization needs to be included in future studies. The metabolic data also suggested that allosteric inhibition occurred under photoautotrophic conditions. It has been reported that cyanobacteria store excess carbons as organic acids in the TCA cycle (Maruyama et al., 2019; Osanai et al., 2014). The result of this study suggested that the possible role of allosteric inhibition was the down-regulation of the carbon fixation pathway under excess carbon conditions (Fig. 4c). Prk was recently identified as an important target for the metabolic engineering of cyanobacteria. The overexpression of Prk protein was

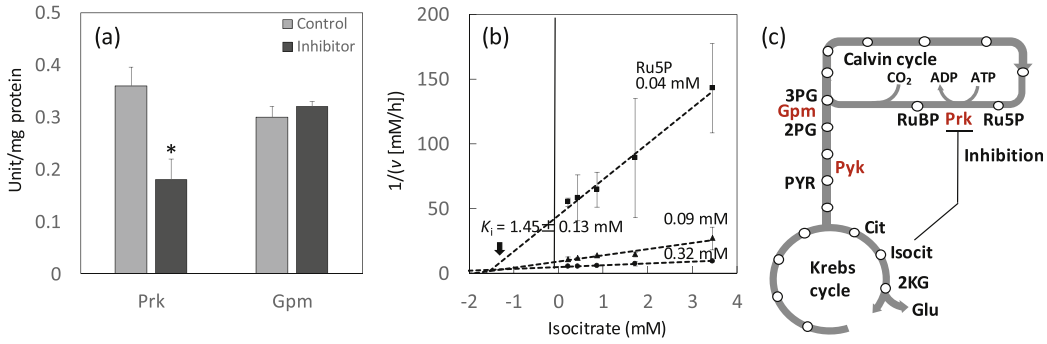

Fig. 4. Enzyme assay of phosphoribulokinase (Prk) and phosphoglycerate mutase (Gpm) from *Synechocystis* sp. PCC 6803. (a) Inhibition of Prk by the addition of 1.7 mM isocitrate, and inhibition of Gpm by the addition of 1.0 mM α-ketoglutarate. *$p < 0.05$ (two-sided *t*-test, n = 3). (b) Dixon-plot for inhibition of Prk by isocitrate. All data are presented as mean ± SD (n = 3). (c) Allosteric inhibition identified in this study.

demonstrated to improve the production of bioalcohols significantly but slightly (Kanno et al., 2017; Nishiguchi et al., 2019). The results of this study suggest that further identification of allosteric control and their release would be effective in metabolic engineering of cyanobacteria.

CRediT authorship contribution statement

Hiroki Nishiguchi: Methodology, Investigation, Writing - original draft. **James Liao:** Supervision, Methodology. **Hiroshi Shimizu:** Conceptualization, Supervision. **Fumio Matsuda:** Methodology, Software, Investigation, Writing - original draft, Writing - review & editing.

Declaration of competing interest

The authors declare that they have no known competing financial interests or personal relationships that could have appeared to influence the work reported in this paper.

Acknowledgments

We thank Prof. Eiichiro Fukusaki, Yoshihiro Toya, Dr. Masakazu Toyoshima (Osaka University), and Dr. Taito Ogura (Shimadzu Co.) for helpful comments on this manuscript and for providing technical support for the targeted proteome analysis. This work was supported in part by Grants-in-Aid for Scientific Research (grant numbers 16H06552, 16H06559, and 17H06303), MEXT, Japan and by Strategic International Collaborative Research Program, SICORP for JP-US Metabolomics, JST, Japan.

Appendix A. Supplementary data

Supplementary data to this article can be found online at https://doi.org/10.1016/j.mec.2020.e00153.

6. Research data

All data used in this study were available from Supplementary Figures and Tables. The Python script and model definition file can be downloaded from our GitHub repository: https://github.com/fumiomatsuda/ensemblemodeling.

References

Angermayr, S.A., Gorchs Rovira, A., Hellingwerf, K.J., 2015. Metabolic engineering of cyanobacteria for the synthesis of commodity products. Trends Biotechnol. 33, 352–361.

Bereman, M.S., MacLean, B., Tomazela, D.M., Liebler, D.C., MacCoss, M.J., 2012. The development of selected reaction monitoring methods for targeted proteomics via empirical refinement. Proteomics 12, 1134–1141.

Carrieri, D., Lombardi, T., Paddock, T., Cano, M., Goodney, G.A., Nag, A., Old, W., Maness, P.-C., Seibert, M., Ghirardi, M., Yu, J., 2017. Transcriptome and proteome analysis of nitrogen starvation responses in Synechocystis 6803 ΔglgC, a mutant incapable of glycogen storage. Algal Research 21, 64–75.

Christodoulou, D., Link, H., Fuhrer, T., Kochanowski, K., Gerosa, L., Sauer, U., 2018. Reserve flux capacity in the pentose phosphate pathway enables *Escherichia coli*'s rapid response to oxidative stress. Cell Syst 6, 569–578 e7.

Contador, C.A., Rizk, M.L., Asenjo, J.A., Liao, J.C., 2009. Ensemble modeling for strain development of L-lysine-producing *Escherichia coli*. Metab. Eng. 11, 221–233.

Dash, S., Khodayari, A., Zhou, J., Holwerda, E.K., Olson, D.G., Lynd, L.R., Maranas, C.D., 2017. Development of a core *Clostridium thermocellum* kinetic metabolic model consistent with multiple genetic perturbations. Biotechnol. Biofuels 10, 108.

Flamholz, A., Noor, E., Bar-Even, A., Milo, R., 2012. eQuilibrator—the biochemical thermodynamics calculator. Nucleic Acids Res. 40, D770–D775.

Hirokawa, Y., Matsuo, S., Hamada, H., Matsuda, F., Hanai, T., 2017. Metabolic engineering of *Synechococcus elongatus* PCC 7942 for improvement of 1,3-propanediol and glycerol production based on in silico simulation of metabolic flux distribution. Microb. Cell Factories 16, 212.

Jazmin, L.J., Xu, Y., Cheah, Y.E., Adebiyi, A.O., Johnson, C.H., Young, J.D., 2017. Isotopically nonstationary ^{13}C flux analysis of cyanobacterial isobutyraldehyde production. Metab. Eng. 42, 9–18.

Kanno, M., Carroll, A.L., Atsumi, S., 2017. Global metabolic rewiring for improved CO_2 fixation and chemical production in cyanobacteria. Nat. Commun. 8, 14724.

Khodayari, A., Chowdhury, A., Maranas, C.D., 2014a. Succinate overproduction: a case study of computational strain design using a comprehensive *Escherichia coli* kinetic model. Front Bioeng Biotechnol 2, 76.

Khodayari, A., Maranas, C.D., 2016. A genome-scale *Escherichia coli* kinetic metabolic model k-ecoli457 satisfying flux data for multiple mutant strains. Nat. Commun. 7, 13806.

Khodayari, A., Zomorrodi, A.R., Liao, J.C., Maranas, C.D., 2014b. A kinetic model of *Escherichia coli* core metabolism satisfying multiple sets of mutant flux data. Metab. Eng. 25, 50–62.

Knoop, H., Grundel, M., Zilliges, Y., Lehmann, R., Hoffmann, S., Lockau, W., Steuer, R., 2013. Flux balance analysis of cyanobacterial metabolism: the metabolic network of *Synechocystis* sp. PCC 6803. PLoS Comput. Biol. 9, e1003081.

Knowles, V.L., Smith, C.S., Smith, C.R., Plaxton, W.C., 2001. Structural and regulatory properties of pyruvate kinase from the *Cyanobacterium synechococcus* PCC 6301. J. Biol. Chem. 276, 20966–20972.

Lai, M.C., Lan, E.I., 2015. Advances in metabolic engineering of cyanobacteria for photosynthetic biochemical production. Metabolites 5, 636–658.

Lawrence, B.A., Suarez, C., DePina, A., Click, E., Kolodny, N.H., Allen, M.M., 1998. Two internal pools of soluble polyphosphate in the cyanobacterium *Synechocystis* sp. strain PCC 6308: an in vivo 31P NMR spectroscopic study. Arch. Microbiol. 169, 195–200.

Lee, B.G., Read, B.A., Tabita, F.R., 1991. Catalytic properties of recombinant octameric, hexadecameric, and heterologous cyanobacterial/bacterial ribulose- 1,5-bisphosphate carboxylase/oxygenase. Arch. Biochem. Biophys. 291, 263–269.

Liebermeister, W., Uhlendorf, J., Klipp, E., 2010. Modular rate laws for enzymatic reactions: thermodynamics, elasticities and implementation. Bioinformatics 26, 1528–1534.

Loferer-Krossbacher, M., Klima, J., Psenner, R., 1998. Determination of bacterial cell dry mass by transmission electron microscopy and densitometric image analysis. Appl. Environ. Microbiol. 64, 688–694.

Maruyama, M., Nishiguchi, H., Toyoshima, M., Okahashi, N., Matsuda, F., Shimizu, H., 2019. Time-resolved analysis of short term metabolic adaptation at dark transition in *Synechocystis* sp. PCC 6803. J. Biosci. Bioeng. 128, 424–428.

Matsuda, F., Toya, Y., Shimizu, H., 2017. Learning from quantitative data to understand central carbon metabolism. Biotechnol. Adv. 35, 971–980.

Mohammadi, R., Fallah-Mehrabadi, J., Bidkhori, G., Zahiri, J., Javad Niroomand, M., Masoudi-Nejad, A., 2016. A systems biology approach to reconcile metabolic network models with application to *Synechocystis* sp. PCC 6803 for biofuel production. Mol. Biosyst. 12, 2552–2561.

Nagai, H., Masuda, A., Toya, Y., Matsuda, F., Shimizu, H., 2018. Metabolic engineering of mevalonate-producing *Escherichia coli* strains based on thermodynamic analysis. Metab. Eng. 47, 1–9.
Nakajima, T., Kajihata, S., Yoshikawa, K., Matsuda, F., Furusawa, C., Hirasawa, T., Shimizu, H., 2014. Integrated metabolic flux and omics analysis of *Synechocystis* sp. PCC 6803 under mixotrophic and photoheterotrophic conditions. Plant Cell Physiol. 55, 1605–1612.
Nakajima, T., Yoshikawa, K., Toya, Y., Matsuda, F., Shimizu, H., 2017. Metabolic flux analysis of *Synechocystis* sp. PCC 6803 DnrtABCD mutant reveals a mechanism for metabolic adaptation to nitrogen-limited conditions. Plant Cell Physiol. 58, 537–545.
Namakoshi, K., Nakajima, T., Yoshikawa, K., Toya, Y., Shimizu, H., 2016. Combinatorial deletions of *glgC* and *phaCE* enhance ethanol production in *Synechocystis* sp. PCC 6803. J. Biotechnol. 239, 13–19.
Nishiguchi, H., Hiasa, N., Uebayashi, K., Liao, J., Shimizu, H., Matsuda, F., 2019. Transomics data-driven, ensemble kinetic modeling for system-level understanding and engineering of the cyanobacteria central metabolism. Metab. Eng. 52, 273–283.
Nishino, S., Okahashi, N., Matsuda, F., Shimizu, H., 2015. Absolute quantitation of glycolytic intermediates reveals thermodynamic shifts in *Saccharomyces cerevisiae* strains lacking *PFK1* or *ZWF1* genes. J. Biosci. Bioeng. 120, 280–286.
Oliver, J.W.K., Atsumi, S., 2015. A carbon sink pathway increases carbon productivity in cyanobacteria. Metab. Eng. 29, 106–112.
Oliver, N.J., Rabinovitch-Deere, C.A., Carroll, A.L., Nozzi, N.E., Case, A.E., Atsumi, S., 2016. Cyanobacterial metabolic engineering for biofuel and chemical production. Curr. Opin. Chem. Biol. 35, 43–50.
Osanai, T., Kanesaki, Y., Nakano, T., Takahashi, H., Asayama, M., Shirai, M., Kanehisa, M., Suzuki, I., Murata, N., Tanaka, K., 2005. Positive regulation of sugar catabolic pathways in the cyanobacterium Synechocystis sp. PCC 6803 by the group 2 sigma factor sigE. J. Biol. Chem. 280, 30653–30659.
Osanai, T., Kuwahara, A., Iijima, H., Toyooka, K., Sato, M., Tanaka, K., Ikeuchi, M., Saito, K., Hirai, M.Y., 2013. Pleiotropic effect of sigE over-expression on cell morphology, photosynthesis and hydrogen production in *Synechocystis* sp. PCC 6803. Plant J. : for cell and molecular biology 76, 456–465.
Osanai, T., Oikawa, A., Shirai, T., Kuwahara, A., Iijima, H., Tanaka, K., Ikeuchi, M., Kondo, A., Saito, K., Hirai, M.Y., 2014. Capillary electrophoresis-mass spectrometry reveals the distribution of carbon metabolites during nitrogen starvation in *Synechocystis* sp. PCC 6803. Environ. Microbiol. 16, 512–524.
Raines, C.A., 2011. Increasing photosynthetic carbon assimilation in C3 plants to improve crop yield: current and future strategies. Plant Physiol. 155, 36–42.
Rizk, M.L., Liao, J.C., 2009. Ensemble modeling for aromatic production in *Escherichia coli*. PloS One 4, e6903.
Shastri, A.A., Morgan, J.A., 2005. Flux balance analysis of photoautotrophic metabolism. Biotechnol. Prog. 21, 1617–1626.
Shirai, T., Osanai, T., Kondo, A., 2016. Designing intracellular metabolism for production of target compounds by introducing a heterologous metabolic reaction based on a *Synechosystis* sp. 6803 genome-scale model. Microb. Cell Factories 15, 13.
Spreitzer, R.J., Salvucci, M.E., 2002. Rubisco: structure, regulatory interactions, and possibilities for a better enzyme. Annu. Rev. Plant Biol. 53, 449–475.
Stitt, M., Schulze, D., 1994. Does rubisco control the rate of photosynthesis and plant-growth?an exercise in molecular ecophysiology. Plant Cell Environ. 17, 465–487.
Takeya, M., Hirai, M.Y., Osanai, T., 2017. Allosteric inhibition of phosphoenolpyruvate carboxylases is determined by a single amino acid residue in cyanobacteria. Sci. Rep. 7, 41080.
Takeya, M., Ito, S., Sukigara, H., Osanai, T., 2018. Purification and characterisation of malate dehydrogenase from *Synechocystis* sp. PCC 6803: biochemical barrier of the oxidative tricarboxylic acid cycle. Front. Plant Sci. 9, 947.
Tamoi, M., Miyazaki, T., Fukamizo, T., Shigeoka, S., 2005. The Calvin cycle in cyanobacteria is regulated by CP12 via the NAD(H)/NADP(H) ratio under light/dark conditions. Plant J. 42, 504–513.
Tokumaru, Y., Uebayashi, K., Toyoshima, M., Osanai, T., Matsuda, F., Shimizu, H., 2018. Comparative targeted proteomics of the central metabolism and the photosystems in the *SigE* mutant strains of *Synechocystis* sp. PCC 6803. Mol. Cell 23, 1051.
Tran, L.M., Rizk, M.L., Liao, J.C., 2008. Ensemble modeling of metabolic networks. Biophys. J. 95, 5606–5617.
Tsukamoto, Y., Fukushima, Y., Hara, S., Hisabori, T., 2013. Redox control of the activity of phosphoglycerate kinase in *Synechocystis* sp. PCC6803. Plant Cell Physiol. 54, 484–491.
Wadano, A., Nishikawa, K., Hirahashi, T., Satoh, R., Iwaki, T., 1998. Reaction mechanism of phosphoribulokinase from a cyanobacterium, *Synechococcus* PCC7942. Photosynth. Res. 56, 27–33.
Wedel, N., Soll, J., 1998. Evolutionary conserved light regulation of Calvin cycle activity by NADPH-mediated reversible phosphoribulokinase/CP12/glyceraldehyde-3-phosphate dehydrogenase complex dissociation. Proc. Natl. Acad. Sci. U.S.A. 95, 9699–9704.
Yoshikawa, K., Hirasawa, T., Ogawa, K., Hidaka, Y., Nakajima, T., Furusawa, C., Shimizu, H., 2013. Integrated transcriptomic and metabolomic analysis of the central metabolism of *Synechocystis* sp. PCC 6803 under different trophic conditions. Biotechnol. J. 8, 571–580.
Yoshikawa, K., Toya, Y., Shimizu, H., 2017. Metabolic engineering of *Synechocystis* sp. PCC 6803 for enhanced ethanol production based on flux balance analysis. Bioproc. Biosyst. Eng. 40, 791–796.
Young, J.D., Shastri, A.A., Stephanopoulos, G., Morgan, J.A., 2011. Mapping photoautotrophic metabolism with isotopically nonstationary ^{13}C flux analysis. Metab. Eng. 13, 656–665.